Colicin E1 binds to TolC as an open hinge to penetrate the outer-membrane

Authors: S. Jimmy Budiardjo[1], Jacqueline J. Stevens[2], Anna L. Calkins[3], Ayotunde P. Ikujuni[2], Virangika K. Wimalasena[2], Emre Firlar[4], David A. Case[5], Julie S. Biteen[3], Jason T. Kaelber[4] and Joanna S.G. Slusky[1,2,*]

Affiliations:

[1] Center for Computational Biology, The University of Kansas, 2030 Becker Dr., Lawrence, KS 66047

[2] Department of Molecular Biosciences, The University of Kansas, 1200 Sunnyside Ave. Lawrence KS 66045

[3] Department of Chemistry, University of Michigan, Ann Arbor MI 48109-1055.

[4] Rutgers CryoEM & Nanoimaging Facility and Institute for Quantitative Biomedicine, Rutgers, The State University of New Jersey, Piscataway, NJ 08854, USA

[5] Department of Chemistry and Chemical Biology, Rutgers University, Piscataway, NJ 08854 USA

*Correspondence: slusky@ku.edu.

ABSTRACT

The double membrane architecture of Gram-negative bacteria forms a barrier that is effectively impermeable to extracellular threats. Bacteriocin proteins evolved to exploit the accessible, surface-exposed proteins embedded in the outer membrane to deliver cytotoxic cargo. Colicin E1 is a bacteriocin produced by, and lethal to, *Escherichia coli* that hijacks the outer membrane proteins TolC and BtuB to enter the cell. Here we capture the colicin E1 translocation domain inside its membrane receptor, TolC, by high-resolution cryoEM. Colicin E1 binds stably to TolC as an open hinge through the TolC pore—an architectural rearrangement from colicin E1's unbound conformation. This binding is stable in live *E. coli* cells as indicated by single-molecule fluorescence microscopy. Finally, colicin E1 fragments binding to TolC plugs the channel,

29 inhibiting its native efflux function as an antibiotic efflux pump and heightening susceptibility to
30 four antibiotic classes.

31

32 **INTRODUCTION**

33 In Gram-negative bacteria, the concentric structures of the outer membrane, cell wall, and
34 cytoplasmic membrane protect the cell from extracellular threats. Of these protective structures,
35 the outer membrane forms a particularly formidable barrier[4], owing to the impermeability of the
36 lipopolysaccharide (LPS) layer that constitutes the outer membrane[5]. The primary means by
37 which external molecules can gain access to the cell is through the ~100 varieties of barrel-
38 shaped proteins that are embedded in each bacterium outer membrane[6] and whose diverse
39 functions include the transport of molecules across the membrane—specifically, the import of
40 nutrients and metabolites and the export of toxins and waste.

41 Because outer membrane proteins (OMPs) are accessible from outside the cell,
42 bacteriophage and bacterial toxins have evolved to exploit OMPs to initiate delivering cargo
43 across the outer membrane. Bacteriocins hijack the OMPs of a target bacterium to cross its
44 impermeable outer membrane and kill the bacterium. Colicins are *E. coli*-specific bacteriocins,
45 protein toxin systems through which bacteria engage in bacterial warfare with other, similar
46 bacteria. Although colicins differ in their receptor targets and killing mechanisms, most colicins
47 share a common tri-domain architecture, comprising the following components: (i) an N-terminal
48 translocation (T) domain, (ii) a receptor-binding (R) domain, and (iii) a C-terminal cytotoxic (C)
49 domain (Figure 1A). Much of what is known of E colicin import has been determined through
50 studies of the colicin E3 and E9 as reviewed by Cramer et al.[7] Import is initialized by R domain
51 binding to the vitamin B12 transporter, BtuB, with high affinity[8,9]; this binding localizes the
52 colicin onto the outer membrane. Once the colicin is tethered to the outer membrane surface, the

53 T domain initiates translocation using the secondary OMP receptor OmpF to access TolA/Pal
54 system for group A colicins or the Ton system group B colicins. In most cases, the T domain
55 requires an OMP distinct from the R domain target.[10] A handful of colicins have been
56 structurally characterized with their OMP counterparts, although not in their entirety. Previous
57 structures of short N-terminal fragments of the T domain of ColE9 with OmpF[11] and the The R
58 domains of ColE2/E3 and Ia with BtuB[9,12] and Cir[8], respectively showed that T domains fully
59 penetrate deeply into lumen of the outer membrane receptors while R domains interact with the
60 extracellular loop regions of their receptors. Studies of the bacteriocin pyocin S5 from
61 *Pseudomonas aeruginosa* suggest that bacteriocin architectures and mechanisms may be
62 conserved across all Gram-negative species.

63 Colicin E1 is a bacteriocin secreted by *E. coli* that enters the periplasm of neighboring
64 cells and forms a pore on the cytoplasmic membrane leading to membrane depolarization and
65 cell death. Colicin E1 uses TolC, the outer membrane component of the acridine efflux pump, as
66 the T domain receptor[13] and BtuB as the R domain receptor[14]. A high-resolution x-ray structure
67 exists of only the cytotoxic domain of colicin E1[15] but not the T or R domains, thus no
68 mechanistic insights can be gained about initial steps of import. Domain swapping experiments
69 between colicin A and E1 identified regions of the protein that interact with specific outer
70 membrane proteins. Early studies of pore forming colicins, including E1, showed that cytotoxic-
71 domain-induced K^+ efflux on the inner membrane can be reversed after it has begun by
72 subsequent addition of trypsin to cells. This, in addition to trypsin's inability to cross the outer
73 membrane, led to the belief that portions of colicin remain tethered to their OMP partners as the
74 cytotoxic domain depolarizes the cytoplasmic membrane.[16-19]

75 In order to understand the early stages of colicin E1 import, functional studies of
76 truncations of colicin E1 which lack the cytotoxic domain have been characterized *in vitro*.
77 Residues 100-120 of colicin E1 (termed the 'TolC box', Figure 1A) have been shown to be
78 necessary but not sufficient for binding TolC. Peptides that include the TolC box co-elute with
79 TolC[20] and disrupt channel conductance[20,21]. Moreover, *E. coli* exposure to TolC-box-containing
80 peptides can prevent subsequent binding and cytotoxicity of full-length colicin E1[22]. Circular
81 dichroism of the T domain indicates that it exists as a helical hairpin in solution (similar to other
82 colicin T domains)[23] and that the proline at the center of the TolC box forms its apex[20]. This
83 measurement led to the proposal, known as the "pillar model,"[20] that the T domain inserts into
84 the TolC barrel as a helical hairpin where the N and C-termini are pointing to the cell exterior.
85 According to this model, the hairpin stuck in TolC acts as a buttress to facilitate the cytotoxic
86 domain entry directly through the membrane.
87 A competing model for colicin E1 import, known as the "total thread" model[7,20], posits
88 that the protein unfolds and passes through TolC N-terminus-first as an unstructured peptide,
89 followed by refolding in the periplasm. In this model the binding between the intrinsically
90 unstructured colicin N-termini and periplasmic proteins[22,24] creates a pulling force that results in
91 the translocation of the whole colicin.
92 Here we use cryogenic electron microscopy (cryoEM) to solve the high-resolution
93 structure of the colicin E1 T domain bound to TolC. We find that colicin E1 binds stably to
94 TolC, not as a helical hairpin but as a single-pass folded helix with the N-terminus inside the
95 periplasm. Additionally, we find that the colE1 TR domain binds TolC *in vivo* as well. Using
96 single-molecule fluorescence microscopy, we find that colE1-TR, lacking the cytotoxic domain,
97 remains stalled on the outer membrane and does not fully translocate into cells. Lastly, we

98 leverage this stalling of ColE1 to block the native TolC function as an antibiotic efflux pump.
99 Through real-time efflux assays, minimum inhibitory concentration (MIC) experiments, we find
100 that colE1-TR and colE1-T are able to inhibit TolC-mediated efflux. We find that this plugging
101 of TolC reduces the amount of antibiotics required to inhibit the bacterial growth—indicating
102 that this colicin E1 fragment reduces the antibiotic resistance conferred by TolC.

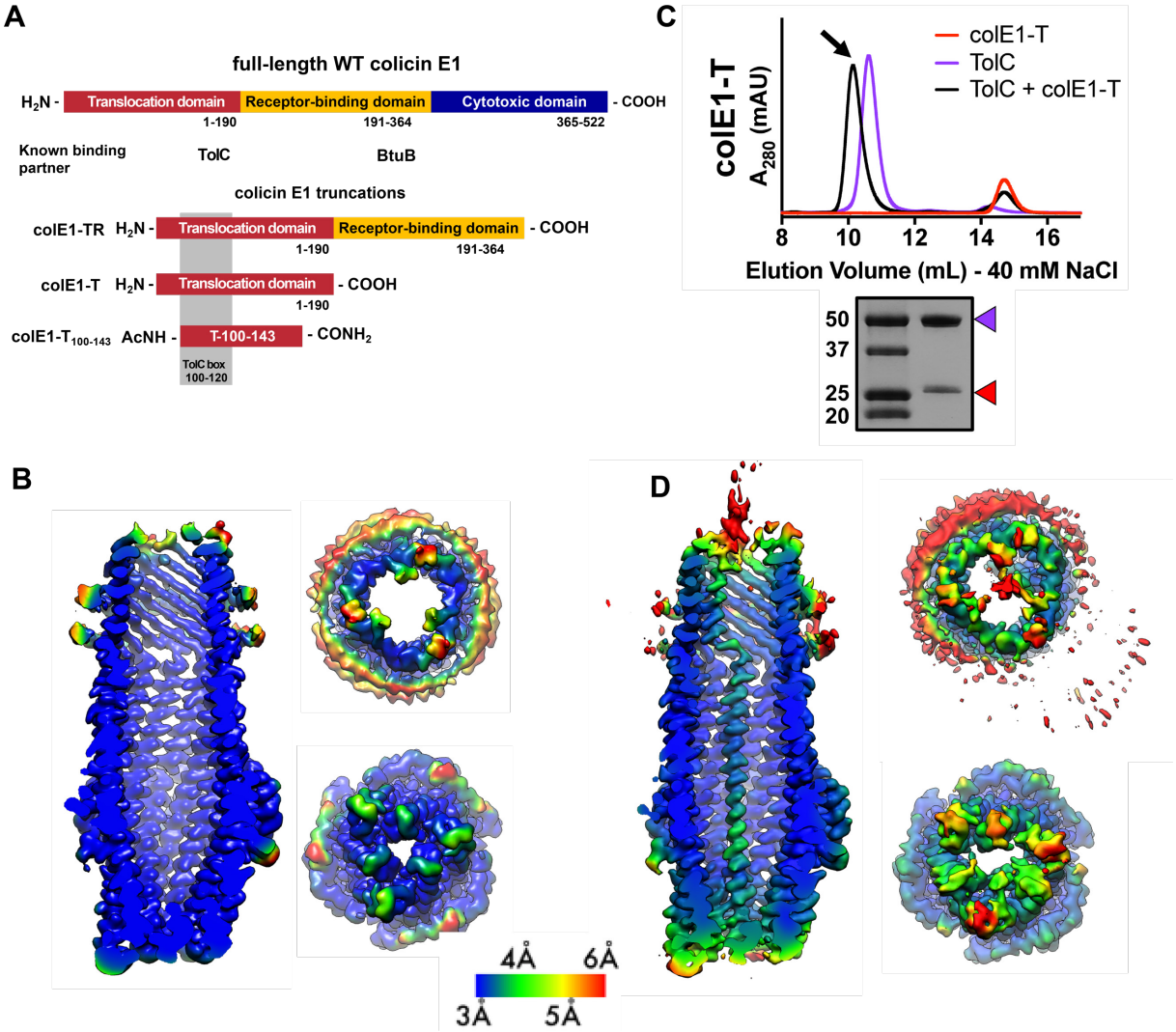

Figure 1. Cell-surface localization of colicin E1 fragments. (A) Architecture of full-length colicin E1 showing domains and their known binding partners. Three truncation constructs used in this study (B) CryoEM structure of TolC embedded in nanodiscs. Side, top, and bottom views are colored by local resolution, as computed in cryoSPARC from the final half-maps. The side view is cropped to display the particle interior. (C) SEC chromatogram of colE1-T (red line) and TolC (purple line). The arrow indicates the co-elution (black line) fractions that were analyzed by SDS-PAGE. On the SDS-PAGE gel (bottom), red arrows indicate the presence of the colicin E1 construct that has co-eluted with TolC. (D) The CryoEM structure of colE1-T bound to TolC and colored by local resolution as in (B).

104 **RESULTS**

105 **CryoEM structure of TolC embedded in nanodiscs**

106 To determine the structural details of colicin E1 binding to TolC, we solved the cryoEM
107 (cryogenic electron microscopy) structure of TolC embedded in nanodiscs with and without
108 added colE1-T (PDB 6WXH and 6WXI, respectively). We recently reported a high-yield TolC
109 preparation by refolding from inclusion bodies[25] and inserted refolded TolC into nanodiscs. The
110 cryoEM structure of refolded TolC alone (Figure 1B) is similar to the previously published
111 crystal structures of natively derived TolC alone[26] or in complex with hexamminecobalt[27] but
112 with more splayed loops at the periplasmic opening (residues 165-175). There was local
113 variation in

114 **Table 1 Cryo-EM data collection, refinement, and validation statistics**

	TolC (EMDB-21960) (PDB 6WXI)	TolC + colE1 (EMDB-21959) (PDB 6WXH)
Data collection and processing		
Electron microscope	Talos Arctica	Talos Arctica
Magnification	130,000×	205,000×
Voltage (kV)	200	200
Electron exposure (e–/Å^2)	33.04	35.96
Defocus range (μm)	0.5-2.6	0.4-2.1
Pixel size (Å)	1.038	0.6578
Symmetry imposed	C_3	C_1 (C_3)
Initial particle images (no.)	2,092,678	339,779
Final particle images (no.)	778,220	179,834
Map resolution (Å) FSC threshold	2.84 0.143	3.09 (2.81) 0.143
Refinement		
Initial model used (PDB code)	6WXH	1TQQ
Model resolution (Å) FSC threshold	3.11 0.5	3.37 0.5

R.m.s. deviations		
Bond lengths (Å)	0.0072	0.012
Bond angles (°)	1.11	1.76
Validation		
MolProbity score	1.33	0.50
Clashscore	4.42	0.00
Poor rotamers (%)	1.40	0.18
Ramachandran plot		
Favored (%)	98.12	98.31
Allowed (%)	1.88	1.32
Disallowed (%)	0	0.37

resolution within the model with lower resolution associated with the extracellular/periplasmic ends and the nanodisc scaffold protein (Figure 1B). The lower residue resolution at these apertures may indicate dynamics not captured in the x-ray crystal structures.

We next determined binding of colicin E1-T domain to capture the complex for structure determination. Residues 1-190 (colE1-T) which span the translocation domain and are known to bind to TolC (Figure 1A). We determined colE1-T:TolC binding *in vitro* via co-elution by size exclusion chromatography (SEC) as previously described[28]. When colE1-T and TolC were mixed, we observed a leftward shift in the TolC peak and a decrease in intensity associated with the colE1-T peak indicating that a subset of the population has migrated with TolC (Figure 1C). We analyzed the peak (Figure 1C arrow) using SDS-PAGE and found the presence of both colE1-T and TolC. The unimodal shifted peak observed with colE1-T:TolC indicates that there is a single species of fully bound TolC. When resolved by cryoEM, addition of colE1-T to TolC breaks the three-fold channel symmetry and the additional protein is observed running all the way through the TolC barrel as a single-pass, all-α-helical chain spanning more than 130 Å (Figure 1D). The maps refined to nominal global resolutions of 2.84 Å and 3.09 Å for the TolC and colE1-T:TolC, respectively (Table 1).

131 The colE1 T domain inserts into TolC with its amino terminus pointing inwards through
132 the periplasmic iris, and 2D class-averages show that the carboxy terminus of the helix continues
133 and projects out into the extracellular space (Figure 2A). 85 of the 190 colE1-T residues could be
134 modeled to this density (residues 46-131) (Figure 2B). No such regular protrusion was seen for
135 the glycine-rich colE1 amino-terminus, which we expect to be disordered in the periplasmic
136 space[20,24,29]. The colE1 chain binds TolC asymmetrically, primarily contacting only one of the
137 three TolC chains.

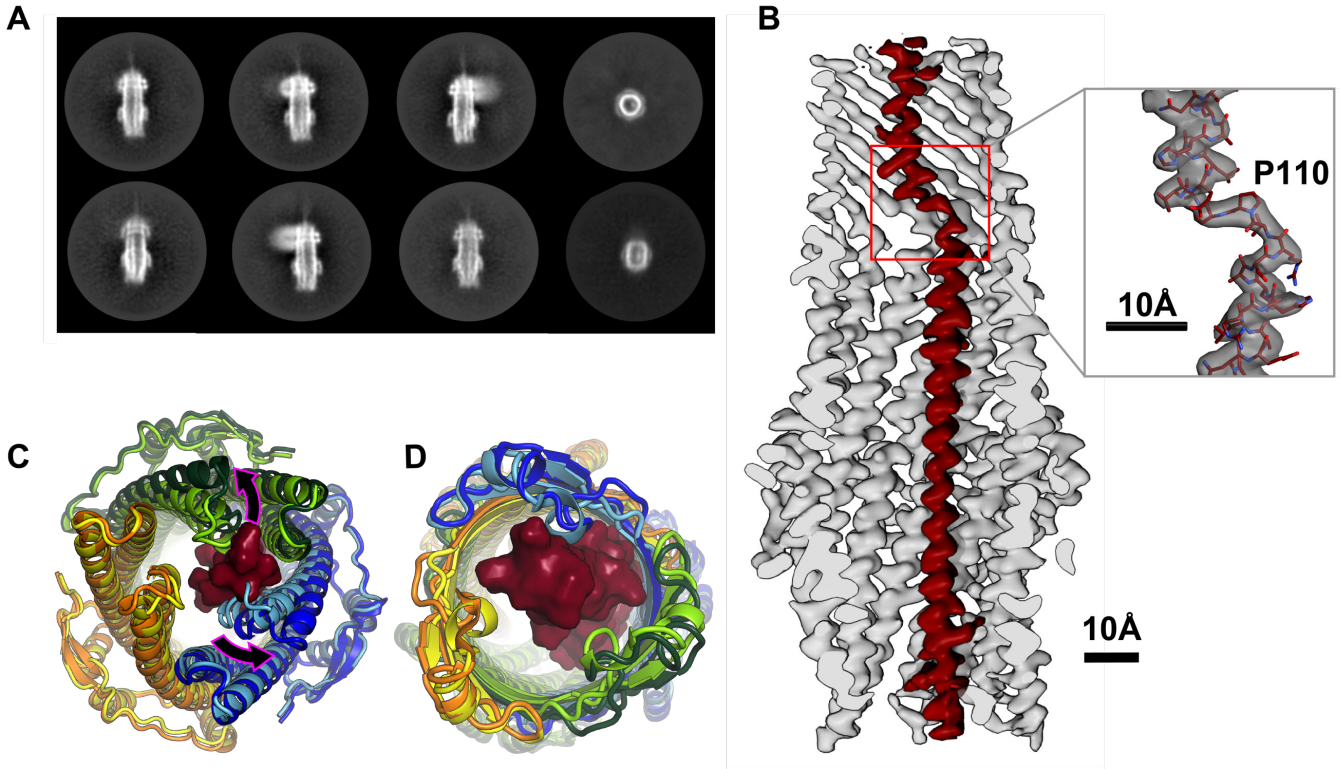

Figure 2. Colicin E1 binds to TolC as a single-pass kinked helix. (A) 2D class averages of colE1-T bound to TolC imbedded in nanodiscs (B) Cutaway view of the TolC interior (gray). ColE1-T (red) binds asymmetrically in an open-hinge conformation. The hinge region of colE1T including P110 shown in stick representation (inset). (C and D) The dilated terminal apertures. The apo cryoEM structure of TolC (subunits colored light blue, light green, and yellow) compared to holo cryoEM structure (subunits colored dark blue, dark green and orange). (C) Periplasmic aperture. (D) Extracellular aperture.

138 Compared to the unbound state, asymmetric colE1 binding dilates the periplasmic TolC
139 aperture (Figure 2C) and, to a lesser extent, the extracellular aperture (Figure 2D) so that they
140 can accommodate colE1 in the absence of any other proteins or motive force. Although the
141 terminal apertures dilate and are filled by the ligand and the TolC box forms specific interactions
142 with the TolC inner wall, the large internal volume of TolC is not fully occupied by colE1.
143 In solution, unbound colicin E1 is a two-helix hairpin as indicated by far UV circular
144 dichroism (CD)[28]. However, our cryoEM reconstruction of colicin E1 in complex with TolC
145 shows that colE1-T hinges open at the TolC box to an extended conformation upon binding to
146 TolC (Figure 2B). The colE1-T helices have a short kink in the middle around proline 110,
147 precisely at the proposed turn location in the hairpin model (Figure 2B inset). This area is also
148 the center of the TolC box that has been known to be critical for the colE1:TolC interaction[20,22].
149

150 **Colicin E1 makes residue-specific interactions with TolC**

151 TolC forms a large rigid conduit in the outer membrane and periplasm (Figure
152 3A) with a water filled lumen. The hydrophilic nature of the channel[30] coupled with the
153 inflexibility of the outer-membrane-embedded barrel largely precludes the formation of any
154 hydrophobic interfaces that are typically the basis of protein-protein interfaces involving helical
155 peptides. Yet, we did observe specific polar contacts between colicin E1's TolC box and the
156 TolC barrel.
157

158 To obtain the most accurate atomic model for interpretation of atomic interactions between

159 peptides, we utilized map-restrained molecular dynamics in model refinement[31]. The refined

160 model had improved chemical plausibility (for instance, MolProbity[32] score improved from 1.25

161 to 0.50) and polar contact were more easily identified. Because this refinement improved the

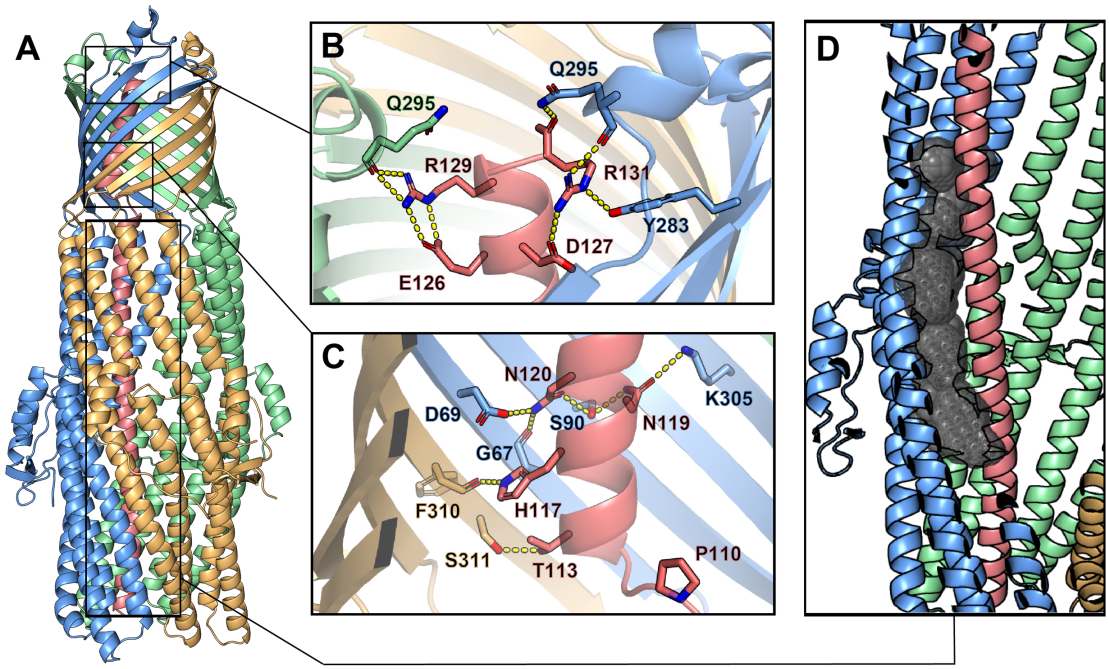

Figure 3. Inter-chain contacts between colE1T and TolC. (A) Molecular dynamics simulation refined structure of the colE1-T:TolC complex colored by chain (colE1-T: light red, TolC: light blue, light green, light gold) (B-C) Polar interaction network of colE1-T and TolC on the C-terminal side of the proline kink in the β-barrel region. (B) near the extracellular opening of TolC and(C) before the transition to the TolC periplasmic helical region. Residues involved in forming polar interactions and proline 110 are shown in sticks. (D) ColE1-T spanning the TolC helical barrel does not make full contact with the side of the TolC barrel. The cavity (black spheres) between colicin (light red) and one chain of TolC (light blue) was detected using GHECOM[1-3]

162 concordance between the map and model, we conclude that the use of cryoEM density as a

163 restraint was successful in preventing overfitting. Specifically, the EMRinger[33] score improved

164 from 2.77 to 3.81 and the map-model FSC=0.5 improved from 3.44Å to 3.37Å.

165 The atomic model showed significant polar interactions form between colicin E1 and

166 TolC at the apertures and around the TolC box. The acidic patch of colicin E1 near the

167 extracellular aperture contains two arginine residues (R129 and R131) that form hydrogen bond
168 networks with one TolC chain each (Figure 3B). In addition, colicin E1 residues T113, A116,
169 N119, N120 (all part of the TolC box) establish polar interactions with TolC residues G67, D69,
170 S90 and K305 on one TolC chain (Figure 3C, light red and light blue) while colicin H117
171 interacts with TolC F310 on a neighboring TolC chain (Figure 3C, light red and light gold). By
172 contrast with the β-barrel of TolC, in the interior of periplasmic helical barrel of TolC, colicin E1
173 does not make full contact with the α-helical barrel interior and there is a gap between the two
174 proteins (Figure 3D). This is in agreement with previous studies that showed a colicin truncation
175 (residues 1-100) that ends just before the beginning of the TolC box does not bind to TolC[20] or
176 prevent cytotoxicity of full-length colicin in cells[22].

177 Moreover, this structure is consistent with reports that mutations at TolC sites G43 or
178 S257 abrogate colE1 activity[34] as these residues are contact sites between TolC and colE1
179 (Figure S1). Conversely, the absence of any effect of mutating colicin R103 and R108[22], is
180 consistent with interaction those residues have with the barrel solvent rather than TolC. The
181 newly solved structure, in combination with previous work[20,22], indicates the specificity of
182 colicin E1 binding to TolC is encoded in the portion that binds to TolC β-barrel.

183 **Membrane localization of colE1 truncations**

184 Since we find the colE1 T domain binds to TolC, we investigated if colicin E1 fragments
185 bind to the native TolC in *E. coli* cells. Though ColE1 C domain activity—depolarizing the inner
186 membrane—requires the C domain to pass through the outer membrane[35], it remains unclear if
187 the colE1-TR domains translocate as well. We first determined *in vitro* binding of colE1-TR,
188 which includes residues 1-364 (colE1-TR) (Figure 1A) which contains the N-terminal portion
189 that binds to TolC and the C-terminal portion that binds to BtuB. ColE1-TR aggregates at the salt

190 concentration (40 mM) used for the co-elution experiment used for colE1-T so we increased the
191 NaCl concentration to 200 mM. ColE1-T still binds to TolC at 250 mM NaCl although to a much
192 lesser degree (Figure S2). Unlike colE1-T (Figure 1C), colE1-TR shows a bimodal distribution
193 indicative of a mixed population of bound and unbound TolC (Figure 4A). Using an extracellular
194 protease digestion assay, we assessed whether colE1-T and colE1-TR translocate into the cell or
195 localize on the cell surface. ColE1 fragments were incubated with cells, washed, and treated with
196 or without trypsin to digest any extracellularly bound protein to cells. When probing for the C-
197 terminal epitope by immunoblotting, there was no detectible colE1-T binding (Figure 4B, left),
198 though there was detectible binding of ColE1-TR (Figure 4B, right). Moreover, we found that if
199 colE1-TR is incubated with cells and subsequently treated with increasing trypsin concentrations,
200 the colE1-TR band disappeared, indicating that the colicin E1 fragment was localized to the
201 outer membrane surface (Figure 4B, right). The colE1-TR band of the intact cells may be slightly
202 less intense than the colE1 band for lysed cells due to some aggregation and precipitation of the
203 intact cell and proteins bound to it when boiling the whole cells for loading the SDS-PAGE. The
204 periplasmic control SurA was not degraded at any trypsin concentration unless the cells were
205 lysed before trypsin digestion[36].

206 Since the proteolysis experiments are not sensitive enough to detect if only a few
207 molecules have entered the cell, we further probed the interaction between the cell membrane
208 and surface-localized colE1-TR with single-molecule fluorescence microscopy using the
209 fluorescent dye Cy3. This method is able to detect single molecules on the cell surface as well as
210 those within the cell indicative of those molecules having crossed the outer membrane[37,38]. When
211 colE1-TR-Cy3 was added to the extracellular environment of WT BW25113 *E. coli* (containing
212 TolC), distinct puncta (Figure 4C, left) formed on 94% of the cells (n = 111) (Figure 4D). In a
213 Δ*tolC* strain, puncta were observed on only 18% of cells (n = 99) (Figure 4C, right; Figure 4D).
214 As a Δ*btuB* control strain, we used BL21 (DE3) which is known to have a premature stop codon
215 at *btuB* residue 58[39]. Puncta were observed on only 3% of cells lacking BtuB (n = 105) (Figure
216 4D and S3A. In WT and Δ*tolC* cells that featured puncta, colE1-TR formed puncta consistent

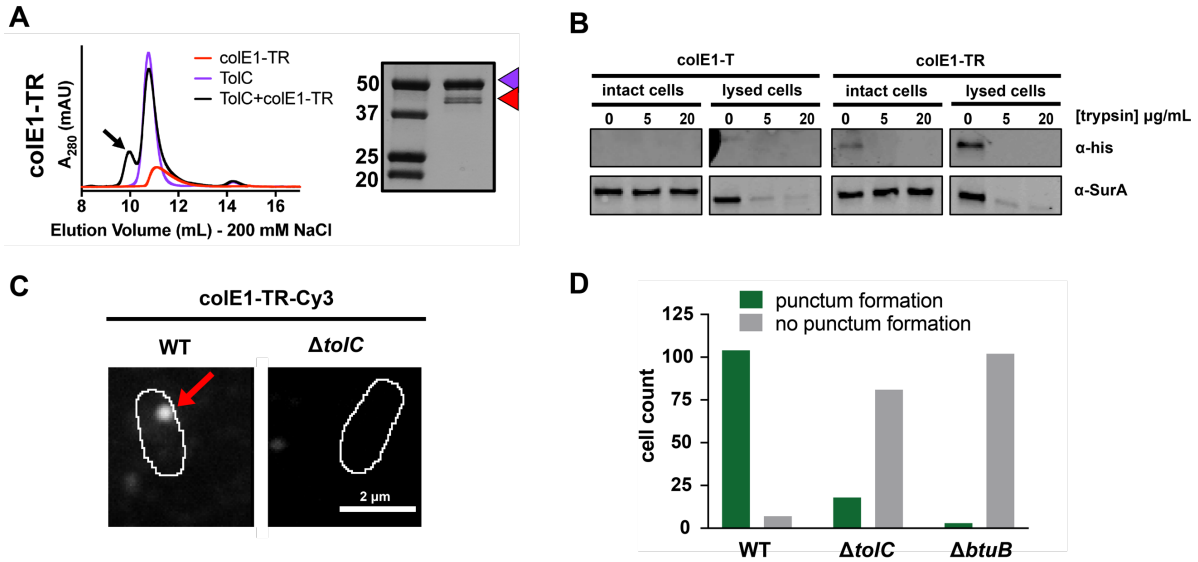

Figure 4. Colicin E1-TR localizes on the outside of the cell. (A) SEC chromatogram of colE1-TR (red line) and TolC (purple line). The arrow indicates the co-elution (black line) fractions that were analyzed by SDS-PAGE. On the SDS-PAGE gels (right), red arrow indicates the presence of colicin E1 construct that has co-eluted with TolC (purple arrow). (B) Extracellular protease digestion assay with two colicin E1 truncation constructs, each labeled with a C-terminal His-Tag. Periplasmic SurA was used as a membrane integrity control. (C) Fluorescence image of colE1-TR-Cy3 overlaid on outlines of living *E. coli* cells for WT and Δ*tolC*. Red arrow points to a punctum. (D) Cell counts where colE1-TR-Cy3 punctum formation was observed for WT, Δ*tolC*, and Δ*btuB*.

217 with ~20 molecules. The observed size and number of molecules are in agreement with previous
218 studies of BtuB puncta[40,41]. To rule out punctum formation as an artifact of Cy3 conjugation, we
219 found colE1-TR-GFP displayed the same cluster formation as colE1-TR-Cy3 (Figure S3B). No
220 other single protein binding events were detected aside from the puncta on either WT or Δ*tolC*
221 cells.

222 Fluorescently labeled pyocins, the colicin analog in *Pseudomonas*, have previously been
223 used to detect translocation across the outer membrane of *Pseudomonas aeruginosa*[42]. Here we
224 use an analogous experiment with fluorescently labeled colE1 to determine cellular localization
225 in *E. coli*. In time courses, bound colE1-TR puncta remained immobile for > 5 minutes (Movie
226 S1). This is consistent with continued association of colE1-TR with membrane-embedded BtuB,
227 which has limited mobility[43]. This result indicates that colE1-TR does not fully translocate[42],
228 because if colE1-TR entered the periplasmic space it would freely diffuse on these timescales.

229 Colicin constructs lacking the R domain (colE1-T-Cy3) showed no detectable binding
230 either to WT or Δ*tolC* cells (Figure S3C), indicating that the TolC-colE1-T interaction is much
231 weaker than the BtuB-colE1-TR interaction.

232 Because we only see one punctum per cell, we anticipate that some BtuB and TolC
233 remain unbound because of the geometric constraints of punctum formation. Though BtuB and
234 TolC need to be in close proximity for colE1 binding to occur, when BtuB clusters together in
235 groups of 12 or more, it may exclude TolC. These cluster geometries would therefore lower the
236 number of full binding sites available for the T and R domains of colicin E1.
237

238 **ColE1-TR inhibits efflux and makes *E. coli* more susceptible to antibiotics**

239 Since the colicin truncations are stalled on their respective OMP receptors, we

240 investigated if this stalling could disrupt native TolC efflux. Real-time efflux inhibition by

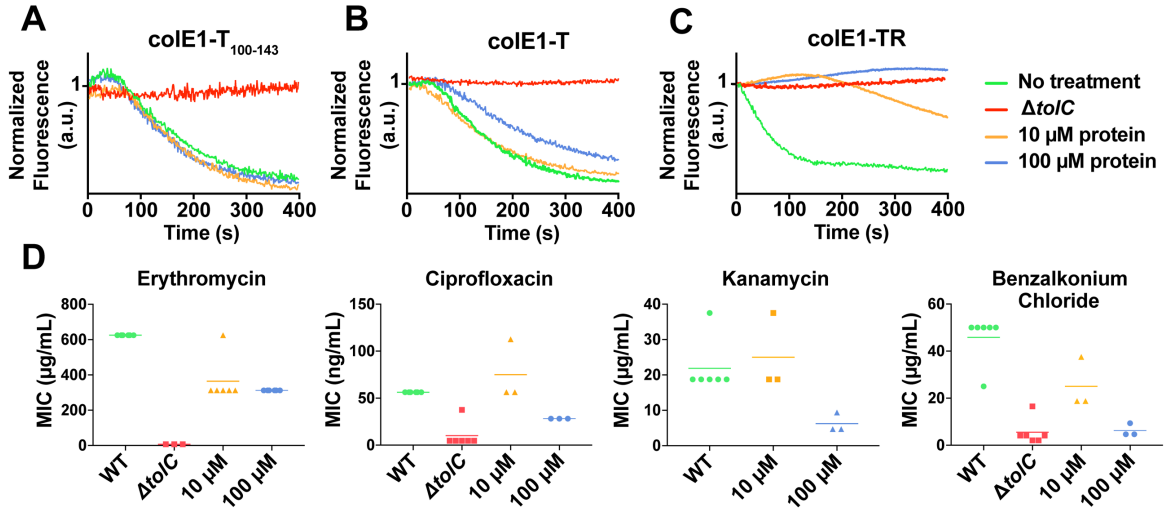

Figure 5. Colicin E1 fragments inhibit efflux and potentiate antibiotics.
(A-C) Effect of colicin E1 fragments on efflux: WT with no protein (green), Δ*tolC* (red), WT + 10 μM (orange), WT + 100 μM protein (blue). (A) colE1-$T_{100\text{-}143}$, (B) colE1-T, (C) colE1-TR. (D) Antibiotic susceptibilities in the absence (green) and presence of colE1-TR added to WT at 10 μM (orange) and 100 μM (blue). MICs for Δ*tolC* (red) are included as a reference. Data are biological replicates reported as the mean and individual data points.

241 colicin E1 fragments was assessed using a live-cell assay with N-(2-naphthyl)-1-naphthylamine

242 (NNN)-dye, which is effluxed by the acridine efflux pump and fluoresces when it is localized

243 inside the cell[44]. NNN efflux can be turned off by the protonophore CCCP, which neutralizes the

244 proton motive force and allows NNN to accumulate within the cell. Active efflux can then be

245 monitored by the fluorescence decay once proton motive force is reenergized by glucose

246 addition[44-48].

247 We assessed the ability of colicin E1 truncations to plug TolC by monitoring real-time

248 NNN efflux. Cells exposed to colE1-$T_{100\text{-}143}$ did not show lower real-time efflux than untreated

249 cells (Figure 5A). This observation is notable in light of the fact that, in previous conductance
250 studies, similar peptides were shown to bind TolC[22,28] and to occlude the channel[21,28].
251 Cells exposed to colE1-T showed less decay in final fluorescence than untreated cells,
252 indicating that colE1-T partially inhibits efflux (Figure 5B). Finally, exposure to colE1-TR
253 produced no decrease in fluorescence, showing full inhibition of efflux (Figure 5C).
254 Because colE1-TR completely inhibits NNN efflux, we evaluated the capacity of colE1-
255 TR to potentiate antibiotics representing four different classes that are known TolC substrates:
256 kanamycin, ciprofloxacin, erythromycin, and benzalkonium chloride (from aminoglycosides,
257 fluoroquinolones, macrolides, and quaternary ammonium compounds, respectively). An effective
258 TolC plug will reduce the concentration required to inhibit growth as antibiotics remain trapped
259 within the cell. WT *E. coli* cells that were exposed to 100 μM colE1-TR with each of these
260 antibiotics showed significantly lower minimum inhibitory concentrations (MICs), the lowest
261 concentration of antibiotic that inhibits visible growth, than cells exposed to the antibiotics alone
262 (Fig. 5D): exposure to 100 μM colE1-TR made WT *E. coli* ~2 to 7-fold more susceptible to these
263 antibiotics (Table S1). Engagement of TolA by the N-terminal TolA box of colicin E9 has
264 previously been shown to cause outer membrane defects[49] which would lead to enhanced
265 antibiotic susceptibility. To rule out outer membrane-mediated defects caused by the TolA box in
266 colE1, we created a truncation of colE1-TR (colE1-TR$_{\Delta 1\text{-}40}$) lacking the N-terminal 40 residues
267 including the TolA box. The MIC of colE1-TR and colE1-TR$_{\Delta 1\text{-}40}$ are identical (Figure S4)
268 indicating that colE1-TR engagement of TolA does not contribute to the observed antibiotic
269 susceptibility.

Discussion

There are two conflicting models of colE1 translocation: 1) the total thread model in which the entire colicin unfolds and threads through TolC[22,50] and 2) the pillar model, in which colicin E1 inserts into TolC as a helical hairpin, facilitating LPS-mediated self-translocation of the colicin cytotoxic domain[28]. Our data support aspects of both models. The belief in a closed hinge conformation of bound colE1 prompted two arguments against the total thread mechanism: 1) the colE1-T closed hinge conformation is too wide to fit through TolC and 2) both ends would face the extracellular milieu[28,50]. The unanticipated colE1-T hinge opening in the bound state resolves these objections: colicin threads into the TolC barrel with the amino terminus pointing into the periplasm, as the total thread model hypothesized. However, our trypsin digests and single-molecule fluorescence images show colE1-TR stalls at the outer membrane. Though we cannot exclude the possibility that full length protein translocation depends on the C domain, we observe—as hypothesized by the pillar model—that colicin sits inside TolC but does not translocate. However, the architecture of the complex differs from that hypothesized by the pillar model. These results are in agreement with early studies of pore-forming colicins in which trypsin added to the extracellular environment can reverse colicin activity. Digestibility by trypsin, as well as the ability of colE1-T/TolC to reconstitute a monodisperse stable complex *in vitro* are consistent with the colicin remain in in contact with its outer membrane receptors while the cytotoxic domain depolarizes the inner membrane.

In addition to demonstrating a colicin insertion mechanism, our observations form the basis of a means to manipulate bacterial import and efflux. Though colicin E1 confers some level of antibiotic potentiation, the relatively high concentration of colE1-TR needed to inhibit efflux may be explained by a combination of the geometric constraints of creating large clusters of

293 BtuB and TolC, low colE1-T-TolC affinity[51], and residually unblocked pore, even in the bound
294 state. Because of their limited potency, our colE1-T and colE1-TR fragments are not likely to be
295 practical in direct applications of antibiotic potentiation. However, our proof-of-concept findings
296 offer a potential roadmap for further development. A more potent TolC binder would not need
297 the R domain anchor for affinity. Such a binder could be designed using the atomic details of the
298 colE1-T-TolC structure as a basis. Moreover, this scaffold can be used for efflux pump inhibitors
299 for at least five other bacterial organisms. Each of these organisms has a structurally
300 characterized outer membrane efflux pump that is homologous and structurally similar to TolC[52].

301 More broadly, there are at least nine known outer membrane protein receptors for
302 bacteriocins. These outer membrane proteins have a variety of functions including adhesion, iron
303 transport, and general import[10,53]. Using this same strategy with fragments derived from other
304 bacteriocins may additionally allow for controlled inhibition of other bacterial functions.

305 **Acknowledgments** We gratefully acknowledge Daniel Montezano, Pinakin Sukthankar, Rik
306 Dhar, Dwight Deay, Scott Lovell, Matthias Wolf, Alexander Little, and Heather Shinogle for
307 discussions and feedback, Mark Richter for the use of his fluorometer, Rajeev Misra for the pTrc
308 vector containing the TolC gene, Vasileios Petrou for guidance on nanodiscs, Chamani Perera
309 for peptide synthesis, Karen Marom for editorial guidance. We thank the Office of Advanced
310 Research computing (OARC) at Rutgers for high-performance computing resources. Funding:
311 NIH award R21-GM128022 to JSB, NIGMS awards DP2GM128201, P20GM113117,
312 P20GM103638 and the Gordon and Betty Moore Inventor Fellowship to JSGS, and NIGMS
313 awards P20 GM103418 and 2K12GM063651 to SJB.

314 **Author contributions** Conceptualization: SJB, JSGS; Methodology: SJB, JTK, JSGS, JSB;
315 Writing: SJB, JSGS, JSB, JTK; Editing: SJB, JSGS, JSB, JTK; Investigation: SJB, JJS, ALC,
316 API, VKW, EF, DAC, and JTK.

317 **Competing interests** The authors declare no competing interests.

318
319

References

1. Kawabata, T. Detection of multiscale pockets on protein surfaces using mathematical morphology. *Proteins* **78**, 1195-211 (2010).
2. Kawabata, T. Detection of cave pockets in large molecules: Spaces into which internal probes can enter, but external probes from outside cannot. *Biophys Physicobiol* **16**, 391-406 (2019).
3. Kawabata, T. & Go, N. Detection of pockets on protein surfaces using small and large probe spheres to find putative ligand binding sites. *Proteins* **68**, 516-29 (2007).
4. Alexander, C. & Rietschel, E.T. Invited review: Bacterial lipopolysaccharides and innate immunity. *Journal of Endotoxin Research* **7**, 167-202 (2001).
5. Kamio, Y. & Nikaido, H. Outer membrane of Salmonella typhimurium: accessibility of phospholipid head groups to phospholipase c and cyanogen bromide activated dextran in the external medium. *Biochemistry* **15**, 2561-70 (1976).
6. Freeman, J.T.C. & Wimley, W.C. TMBB-DB: a transmembrane β-barrel proteome database. *Bioinformatics* **28**, 2425-2430 (2012).
7. Cramer, W.A., Sharma, O. & Zakharov, S.D. On mechanisms of colicin import: the outer membrane quandary. *Biochem J* **475**, 3903-3915 (2018).
8. Buchanan, S.K. et al. Structure of colicin I receptor bound to the R-domain of colicin Ia: implications for protein import. *EMBO J* **26**, 2594-604 (2007).
9. Kurisu, G. et al. The structure of BtuB with bound colicin E3 R-domain implies a translocon. *Nat Struct Biol* **10**, 948-54 (2003).
10. Cascales, E. et al. Colicin Biology. *Microbiology and Molecular Biology Reviews* **71**, 158-229 (2007).
11. Housden, N.G. et al. Directed epitope delivery across the Escherichia coli outer membrane through the porin OmpF. *Proc Natl Acad Sci U S A* **107**, 21412-7 (2010).
12. Sharma, O. et al. Structure of the complex of the colicin E2 R-domain and its BtuB receptor. The outer membrane colicin translocon. *J Biol Chem* **282**, 23163-70 (2007).
13. Benedetti, H. et al. Individual domains of colicins confer specificity in colicin uptake, in pore-properties and in immunity requirement. *J Mol Biol* **217**, 429-39 (1991).
14. Benedetti, H. et al. Comparison of the Uptake Systems for the Entry of Various BtuB Group Colicins into Escherichia coli. *Microbiology* **135**, 3413-3420 (1989).
15. Elkins, P., Bunker, A., Cramer, W.A. & Stauffacher, C.V. A mechanism for toxin insertion into membranes is suggested by the crystal structure of the channel-forming domain of colicin E1. *Structure* **5**, 443-58 (1997).
16. Plate, C.A. & Luria, S.E. Stages in colicin K action, as revealed by the action of trypsin. *Proc Natl Acad Sci U S A* **69**, 2030-4 (1972).
17. Dankert, J., Hammond, S.M. & Cramer, W.A. Reversal by trypsin of the inhibition of active transport by colicin E1. *J Bacteriol* **143**, 594-602 (1980).
18. Dankert, J.R., Uratani, Y., Grabau, C., Cramer, W.A. & Hermodson, M. On a domain structure of colicin E1. A COOH-terminal peptide fragment active in membrane depolarization. *J Biol Chem* **257**, 3857-63 (1982).
19. Benedetti, H., Lloubes, R., Lazdunski, C. & Letellier, L. Colicin A unfolds during its translocation in Escherichia coli cells and spans the whole cell envelope when its pore has formed. *EMBO J* **11**, 441-7 (1992).
20. Zakharov, S.D., Wang, X.S. & Cramer, W.A. The Colicin E1 TolC-Binding Conformer: Pillar or Pore Function of TolC in Colicin Import? *Biochemistry* **55**, 5084-94 (2016).

366 21. Zakharov, S.D. et al. Colicin occlusion of OmpF and TolC channels: outer membrane
367 translocons for colicin import. *Biophys J* **87**, 3901-11 (2004).
368 22. Jakes, K.S. The Colicin E1 TolC Box: Identification of a Domain Required for Colicin
369 E1 Cytotoxicity and TolC Binding. *J Bacteriol* **199**(2017).
370 23. Wiener, M., Freymann, D., Ghosh, P. & Stroud, R.M. Crystal structure of colicin Ia.
371 *Nature* **385**, 461-4 (1997).
372 24. Housden, N.G. et al. Intrinsically disordered protein threads through the bacterial outer-
373 membrane porin OmpF. *Science* **340**, 1570-4 (2013).
374 25. Budiardjo, S.J. et al. High-Yield Preparation of Outer Membrane Protein Efflux Pumps
375 by in Vitro Refolding is Concentration Dependent. *J Membr Biol* **254**, 41-50 (2021).
376 26. Koronakis, V., Sharff, A., Koronakis, E., Luisi, B. & Hughes, C. Crystal structure of the
377 bacterial membrane protein TolC central to multidrug efflux and protein export. *Nature*
378 **405**, 914-9 (2000).
379 27. Higgins, M.K. et al. Structure of the ligand-blocked periplasmic entrance of the bacterial
380 multidrug efflux protein TolC. *J Mol Biol* **342**, 697-702 (2004).
381 28. Zakharov, S.D., Wang, X.S. & Cramer, W.A. The Colicin E1 TolC-Binding Conformer:
382 Pillar or Pore Function of TolC in Colicin Import? *Biochemistry* **55**, 5084-5094 (2016).
383 29. Housden, N.G. et al. Directional Porin Binding of Intrinsically Disordered Protein
384 Sequences Promotes Colicin Epitope Display in the Bacterial Periplasm. *Biochemistry*
385 **57**, 4374-4381 (2018).
386 30. Dhar, R., Feehan, R. & Slusky, J.S.G. Membrane Barrels Are Taller, Fatter, Inside-Out
387 Soluble Barrels. *J Phys Chem B* **125**, 3622-3628 (2021).
388 31. Wu, X., Subramaniam, S., Case, D.A., Wu, K.W. & Brooks, B.R. Targeted
389 conformational search with map-restrained self-guided Langevin dynamics: application
390 to flexible fitting into electron microscopic density maps. *J Struct Biol* **183**, 429-440
391 (2013).
392 32. Williams, C.J. et al. MolProbity: More and better reference data for improved all-atom
393 structure validation. *Protein Sci* **27**, 293-315 (2018).
394 33. Barad, B.A. et al. EMRinger: side chain-directed model and map validation for 3D cryo-
395 electron microscopy. *Nat Methods* **12**, 943-6 (2015).
396 34. Masi, M., Vuong, P., Humbard, M., Malone, K. & Misra, R. Initial steps of colicin E1
397 import across the outer membrane of Escherichia coli. *J Bacteriol* **189**, 2667-76 (2007).
398 35. Brunden, K.R., Uratani, Y. & Cramer, W.A. Dependence of the conformation of a colicin
399 E1 channel-forming peptide on acidic pH and solvent polarity. *J Biol Chem* **259**, 7682-7
400 (1984).
401 36. Besingi, R.N. & Clark, P.L. Extracellular protease digestion to evaluate membrane
402 protein cell surface localization. *Nat Protoc* **10**, 2074-80 (2015).
403 37. Tuson, H.H. & Biteen, J.S. Unveiling the inner workings of live bacteria using super-
404 resolution microscopy. *Anal Chem* **87**, 42-63 (2015).
405 38. Al-Husini, N. et al. BR-Bodies Provide Selectively Permeable Condensates that
406 Stimulate mRNA Decay and Prevent Release of Decay Intermediates. *Mol Cell* **78**, 670-
407 682 e8 (2020).
408 39. Studier, F.W., Daegelen, P., Lenski, R.E., Maslov, S. & Kim, J.F. Understanding the
409 differences between genome sequences of Escherichia coli B strains REL606 and
410 BL21(DE3) and comparison of the E. coli B and K-12 genomes. *J Mol Biol* **394**, 653-80
411 (2009).

412 40. Rassam, P. et al. Supramolecular assemblies underpin turnover of outer membrane
413 proteins in bacteria. *Nature* **523**, 333-6 (2015).
414 41. Chavent, M. et al. How nanoscale protein interactions determine the mesoscale dynamic
415 organisation of bacterial outer membrane proteins. *Nat Commun* **9**, 2846 (2018).
416 42. White, P. et al. Exploitation of an iron transporter for bacterial protein antibiotic import.
417 *Proc Natl Acad Sci U S A* **114**, 12051-12056 (2017).
418 43. Kleanthous, C., Rassam, P. & Baumann, C.G. Protein-protein interactions and the
419 spatiotemporal dynamics of bacterial outer membrane proteins. *Curr Opin Struct Biol* **35**,
420 109-15 (2015).
421 44. Bohnert, J.A., Schuster, S., Szymaniak-Vits, M. & Kern, W.V. Determination of real-
422 time efflux phenotypes in Escherichia coli AcrB binding pocket phenylalanine mutants
423 using a 1,2'-dinaphthylamine efflux assay. *PLoS One* **6**, e21196 (2011).
424 45. Bohnert, J.A., Karamian, B. & Nikaido, H. Optimized Nile Red efflux assay of AcrAB-
425 TolC multidrug efflux system shows competition between substrates. *Antimicrob Agents*
426 *Chemother* **54**, 3770-5 (2010).
427 46. Seeger, M.A. et al. Engineered disulfide bonds support the functional rotation mechanism
428 of multidrug efflux pump AcrB. *Nat Struct Mol Biol* **15**, 199-205 (2008).
429 47. Iyer, R., Ferrari, A., Rijnbrand, R. & Erwin, A.L. A fluorescent microplate assay
430 quantifies bacterial efflux and demonstrates two distinct compound binding sites in AcrB.
431 *Antimicrob Agents Chemother* **59**, 2388-97 (2015).
432 48. Misra, R., Morrison, K.D., Cho, H.J. & Khuu, T. Importance of Real-Time Assays To
433 Distinguish Multidrug Efflux Pump-Inhibiting and Outer Membrane-Destabilizing
434 Activities in Escherichia coli. *J Bacteriol* **197**, 2479-88 (2015).
435 49. Rassam, P. et al. Intermembrane crosstalk drives inner-membrane protein organization in
436 Escherichia coli. *Nat Commun* **9**, 1082 (2018).
437 50. Cramer, W.A., Sharma, O. & Zakharov, S.D. On mechanisms of colicin import: the outer
438 membrane quandary. *Biochemical Journal* **475**, 3903-3915 (2018).
439 51. Taylor, R., Burgner, J.W., Clifton, J. & Cramer, W.A. Purification and characterization of
440 monomeric Escherichia coli vitamin B12 receptor with high affinity for colicin E3. *J Biol*
441 *Chem* **273**, 31113-8 (1998).
442 52. Franklin, M.W. et al. Efflux Pumps Represent Possible Evolutionary Convergence onto
443 the beta-Barrel Fold. *Structure* **26**, 1266-1274.e2 (2018).
444 53. Kleanthous, C. Swimming against the tide: progress and challenges in our understanding
445 of colicin translocation. *Nat Rev Microbiol* **8**, 843-8 (2010).
446 54. Hagn, F., Nasr, M.L. & Wagner, G. Assembly of phospholipid nanodiscs of controlled
447 size for structural studies of membrane proteins by NMR. *Nat Protoc* **13**, 79-98 (2018).
448 55. Wiegand, I., Hilpert, K. & Hancock, R.E. Agar and broth dilution methods to determine
449 the minimal inhibitory concentration (MIC) of antimicrobial substances. *Nat Protoc* **3**,
450 163-75 (2008).
451 56. Daury, L. et al. Tripartite assembly of RND multidrug efflux pumps. *Nat Commun* **7**,
452 10731 (2016).
453 57. Weis, F. & Hagen, W.J.H. Combining high throughput and high quality for cryo-electron
454 microscopy data collection. *Acta Crystallogr D Struct Biol* **76**, 724-728 (2020).
455 58. Mastronarde, D.N. Advanced Data Acquisition From Electron Microscopes With
456 SerialEM. . *Microscopy and Microanalysis* **24**, 864-865 (2018).

457 59. Rice, W.J. et al. Routine determination of ice thickness for cryo-EM grids. *J Struct Biol*
458 **204**, 38-44 (2018).
459 60. Budiardjo, S.J. et al. High yield preparation of outer-membrane protein efflux pumps by
460 in vitro refolding is concentration dependent. *bioRxiv*,
461 2020.09.14.296756 (2020).
462 61. Punjani, A., Rubinstein, J.L., Fleet, D.J. & Brubaker, M.A. cryoSPARC: algorithms for
463 rapid unsupervised cryo-EM structure determination. *Nat Methods* **14**, 290-296 (2017).
464 62. Zivanov, J. et al. New tools for automated high-resolution cryo-EM structure
465 determination in RELION-3. *Elife* **7**(2018).
466 63. Rohou, A. & Grigorieff, N. CTFFIND4: Fast and accurate defocus estimation from
467 electron micrographs. *J Struct Biol* **192**, 216-21 (2015).
468 64. Wagner, T. et al. SPHIRE-crYOLO is a fast and accurate fully automated particle picker
469 for cryo-EM. *Commun Biol* **2**, 218 (2019).
470 65. Cardone, G., Heymann, J.B. & Steven, A.C. One number does not fit all: mapping local
471 variations in resolution in cryo-EM reconstructions. *J Struct Biol* **184**, 226-36 (2013).
472 66. Afonine, P.V. et al. Real-space refinement in PHENIX for cryo-EM and crystallography.
473 *Acta Crystallogr D Struct Biol* **74**, 531-544 (2018).
474 67. Croll, T.I. ISOLDE: a physically realistic environment for model building into low-
475 resolution electron-density maps. *Acta Crystallogr D Struct Biol* **74**, 519-530 (2018).
476 68. Emsley, P., Lohkamp, B., Scott, W.G. & Cowtan, K. Features and development of Coot.
477 *Acta Crystallogr D Biol Crystallogr* **66**, 486-501 (2010).
478 69. Maier, J.A. et al. ff14SB: Improving the Accuracy of Protein Side Chain and Backbone
479 Parameters from ff99SB. *J Chem Theory Comput* **11**, 3696-713 (2015).
480 70. Nguyen, H., Roe, D.R. & Simmerling, C. Improved Generalized Born Solvent Model
481 Parameters for Protein Simulations. *J Chem Theory Comput* **9**, 2020-2034 (2013).
482 71. Goddard, T.D. et al. UCSF ChimeraX: Meeting modern challenges in visualization and
483 analysis. *Protein Sci* **27**, 14-25 (2018).
484

485 **RESOURCE AVAILABILITY**

486 **STAR METHODS**

487 **KEY RESOURCES TABLE**

REAGENT or RESOURCE	SOURCE	IDENTIFIER
Antibodies		
THE HisTag mAb Mouse	GenScript	Cat#A00186-100; RRID:19J001957
anti-SurA Rabbit polyclonal	Cusabio	Cat#CSB-PA359693HA01ENV; RRID:E0109A
IRDye 800CW goat anti-mouse IgG secondary	LI-COR	Cat#925-32210; RRID:C81106-01
IRDye 800CW Donkey anti-Rabbit	LI-COR	Cat#925-32213; RRID:C80829-10
Bacterial and Virus Strains		
BW25113	Coli Genetic Stock Center	Cat#7636

JW5503-1	Coli Genetic Stock Center	Cat#11430
BL21(DE3)	Coli Genetic Stock Center	Cat#12504
Chemicals, Peptides, and Recombinant Proteins		
TolC	This paper	N/A
ColE1-T	This paper	N/A
ColE1-TR	This paper	N/A
ColE1-T100-143	This paper	N/A
Deposited Data		
TolC alone map	This paper	EMDB-21960 PDB 6WXI
TolC-colE1-T complex map	This paper	EMDB-21959 PDB 6WXH
Recombinant DNA		
pTrc99a-NoSS-TolC	This paper	Addgene
pET303-colE1-T	This paper	Addgene
pET303-colE1-TR	This paper	Addgene
MSP1D1	Addgene	Cat#20061
Software and Algorithms		
cryoSPARC 2 v2.12	Punjani, Rubinstein et al. 2017	https://cryosparc.com/
phenix v1.14-3260	Afonine, Poon et al. 2018	https://www.phenix-online.org/
serialEM v3.7	Mastronarde 2018	https://bio3d.colorado.edu/SerialEM/
coot v0.8.9.2-re 7766	Emsley, Lohkamp et al. 2010	https://www2.mrc-lmb.cam.ac.uk/personal/pemsley/coot/
ISOLDE v1.0b4.dev1	Croll 2018	https://isolde.cimr.cam.ac.uk/static/isolde/doc/tools/ISOLDE.html
UCSF ChimeraX	Goddard, Huang et al. 2018	https://www.cgl.ucsf.edu/chimerax/
PyMOL	Schrödinger, LLC	https://pymol.org/2/

RESOURCE AVAILABILITY

Lead Contact

Further information and requests for resources should be directed to and will be fulfilled by the Lead Contact, Joanna Slusky (slusky@ku.edu).

Data and materials availability

All strains used are commercially available. All plasmids available through Addgene. CryoEM maps and models have been deposited with accession codes EMD-21960, EMD-21959, PDB ID 6WXI, and PDB ID 6WXH. All other data is available in the main text or the supplementary materials.

498 **METHOD DETAILS**
499 ***E. coli* strains.** *E. coli* strains BW25113 and JW5503-1 were purchased from the Coli Genetic
500 Stock Center (CGSC). JW5503-1 is a tolC732(del)::kan from the parent strain BW25113.
501 BL21(DE3) were used for expression of the colicin constructs and TolC. BL21(DE3) has a
502 premature stop codon at residue 58 of the *btuB* gene and therefore we used it as a Δ*btuB* strain
503 for microscopy.
504
505 **Expression and Purification**. The gene for colE1-TR was synthesized as a gBlock (Integrated
506 DNA Technologies) and cloned into pET303. Inverse PCR was used to delete the R domain and
507 produce colicin E1-T. The gene for colicin E1-TR-GFP was produced by inserting GFP at the C
508 terminus of colE1-TR.
509
510 Plasmids were transformed into *E. coli* BL21(DE3) cells and plated on LB + agar + 100 µg/mL
511 carbenicillin. Single colonies were inoculated into 50 mL LB broth with 100 µg/mL carbenicillin
512 and grown overnight at 37 °C with shaking at 250 r.p.m. Proteins were expressed by inoculating
513 1L of TB supplemented with 0.4% glycerol, 10 mM $MgCl_2$ and 100 µg/mL carbenicillin with 20
514 mL of the overnight culture. The culture was grown at 37 °C to an OD600 of 2.0 and induced
515 with 1 mM IPTG. Expression cultures were then grown at 15 °C for 24 hours and harvested at
516 4,000 g for 30 minutes at 4 °C. Cell pellets were resuspended at 3 mL/g of cell pellet in lysis
517 buffer (TBS, 5 mM $MgCl_2$, 10 mM imidazole, 1mM PMSF, 10 µg/mL DNase, 0.25 mg/mL
518 lysozyme) and lysed via sonication (2 minutes, 2s on, 8s off, 40% amplitude, QSonica Q500
519 with 12.7 mm probe) in an ice bath. Lysates were centrifuged at 4,000 g for 10 minutes to
520 remove un-lysed cells and debris. The supernatant was centrifuged again at 50,400 g in a
521 Beckman Coulter J2-21 for 1 hour at 4 °C. Clarified lysates were applied to a 5 mL HisTrap FF
522 column and purified using an ÄKTA FPLC system with a 20 column volume wash step with
523 binding buffer (TBS, 25 mM imidazole) and eluted using a linear gradient from 0-50% elution
524 buffer (TBS, 500 mM imidazole) in 10 column volumes. Concentrated proteins were loaded onto
525 a HiLoad Superdex 16/60 200 pg gel filtration column and eluted into phosphate buffered saline
526 (PBS) pH 7.4.
527
528 TolC expression and purification was conducted in the same manner for preparation for cryoEM
529 and for SEC. The gene for full-length TolC (a generous gift from R. Misra) was cloned into
530 pTrc99a with the signal sequence deleted for expression into inclusion bodies. Plasmids were
531 transformed into BL21(DE3) and plated on LB + agar + 100 µg/mL carbenicillin. A single
532 colony was picked and grown in LB at 37 °C with shaking at 250 r.p.m. overnight. In the
533 morning, 1L of LB was inoculated with 20 mL of the overnight culture and grown at 37 °C with
534 shaking at 250 r.p.m. until the culture reached an OD600 of 0.6, at which point protein
535 expression was induced with 1mM IPTG for an additional 4 hours. Cells were then harvested at
536 4,000g for 30 minutes at 4 °C. Cell pellets were resuspended in mL of lysis buffer (TBS, 5 mM
537 $MgCl_2$, 0.2 mg/mL lysozyme, 5 µg/mL DNase, 1mM PMSF) at 3 mL/1g of cell pellet and lysed
538 via sonication (4 minutes, 2s on, 8s off, 40% amplitude, QSonica Q500 with 12.7 mm probe) in
539 an ice bath. Cell lysates were centrifuged at 4,000 g for 30 minutes at 4 °C to harvest inclusion
540 bodies. Inclusion body pellets were resuspended in inclusion body wash buffer (20 mM Tris pH
541 8.0, 0.5 mM EDTA, 1% Triton X-100) and centrifuged at 4,000g for 30 minutes at 4 °C. The
542 inclusion body wash was repeated two more times. A final wash was done in 20 mM Tris pH 8.0
543 and inclusion bodies were stored at -20 °C. Inclusion bodies were solubilized in 20 mM Tris pH

544 8.0, 8M urea at 500 μM. N-octylpolyoxyethylene was added to 5 mL of solubilized TolC to a
545 final concentration of 10% detergent and pipetted into a Slide-A-Lyzer G2 dialysis cassette with
546 a 10,000 molecular weight cut off. Refolding was initiated by dialysis in 5L of 20 mM Tris pH
547 8.0, 100 mM NaCl at 4 °C with stirring overnight. TolC was centrifuged at 15,200 g for 10
548 minutes at 4 °C to remove aggregates. The supernatant was filtered through a 0.22 μm filter,
549 concentrated to 2 mL, applied onto a HiLoad 16/60 Superdex 200 pg column on an ÄKTA Pure
550 FPLC system, and eluted with 1.5 column volumes in 20 mM Tris pH 8.0, 100 mM NaCl, 0.05%
551 n-dodecyl-β-D-maltoside. TolC containing fractions were pooled and concentrated to 300 μM in
552 Amicon centrifugal filters with molecular weight cutoff of 30kDa.
553
554 Membrane scaffold protein MSP1D1. MSP1D1 in pET28a was purchased from Addgene and
555 was expressed and purified as previously described[54].
556
557 **Peptide Synthesis.** ColE1-T100-143 was synthesized using standard Fmoc chemistry with a
558 CEM liberty blue microwave peptide synthesizer. The peptides were cleaved using a solution of
559 92.5:2.5:2.5:2.5 TFA:TIPS:H2O:DoDt and the crude peptides where purified using HPLC.
560 Analytical HPLC traces were acquired using an Agilent 1100 quaternary pump and a Hamilton
561 PRP-1 (polystyrene-divinylbenzene) reverse phase analytical column (7 μm particle size, 4 mm x
562 25 cm) with UV detection at 215 nm. The eluents were heated to 45 °C to reduce separation of
563 rotational isomers, and elution was achieved with gradients of water/ acetonitrile (90:10 to 0:100
564 containing 0.1% TFA) over 20 min. Low-resolution mass spectra (LRMS) were obtained using a
565 Waters Micromass ZQ 4000 instrument with ESI+ ionization
566
567 **Extracellular Protease Digestion.** Protein localization after exogenous protein addition to
568 whole cells was determined as previously described[36].
569
570 **Single-Molecule Microscopy.** Cysteine mutations were introduced at the C-terminus before the
571 histidine tag for fluorophore conjugation. These constructs were purified as described in the
572 expression and purification section with the addition of 1 mM TCEP in all buffers. All
573 subsequent steps were performed with limited exposure to light and in amber tubes. Cyanine3
574 (Cy3) maleimide (Lumiprobe) was reconstituted in DMSO. Fluorophore labeling was achieved
575 by mixing a 20-fold molar excess of Cy3 maleimide to protein and incubating overnight at 4 °C.
576 Free dye was removed by gel filtration on a Sephadex NAP-10 G-25 column. Simultaneously to
577 the dye removal, the sample was buffer exchanged into storage buffer (PBS pH 7.4, 1 mM DTT,
578 1 mM EDTA). The degree of labeling was determined spectrophotometrically from the
579 concentrations of the dye and protein solutions using their respective extinction coefficients, ε, as
580 described by their manufacturers or for the proteins as estimated by Expasy ProtParam (Cy3
581 ε548nm = 162,000 L mol-1 cm-1; colE1-T-E192C ε280nm = 9,970 L mol-1 cm-1; colE1-TR-
582 E366C ε280nm = 14,440 L mol-1 cm-1). Labeling efficiencies were ~75% and ~85% for colE1-
583 T-E192C and colE1-TR-E366C, respectively. Protein concentrations were adjusted according to
584 the percentage of labeled protein.
585
586 Cultures of *E. coli* (WT, ΔtolC, or BL21(DE3)) were grown in LB medium at 37 °C with
587 shaking (180 r.p.m.) overnight, then transferred to MOPS minimal medium (Teknova) with 0.2%
588 glycerol and 1.32 mM K_2HPO_4, and grown at 37 °C for 13 h. The sample was transferred to
589 MOPS medium and grown to turbidity at 37 °C overnight. A 1-mL aliquot of culture was

590 centrifuged for 2 min at 4,850 g to pellet the cells. The pellet was washed in 1 mL MOPS and
591 centrifuged a second time. The supernatant was then removed, and the cell pellet was
592 resuspended in 500 µL MOPS. A 1.0 µL droplet of concentrated cells was placed onto a glass
593 slide. Then, a 1.0 µL droplet of 1 µg/mL colicin E1 protein construct stock was added to the
594 cells. The droplet was covered by an agarose pad (1% agarose in MOPS media) and a second
595 coverslip.
596
597 Samples were imaged at room temperature using wide-field epifluorescence microscopy with
598 sensitivity to detect single dye molecules as described previously [37]. Briefly, fluorescence was
599 excited by a 561-nm laser (Coherent Sapphire 560-50) for Cy3 or a 488-nm laser (Coherent
600 Sapphire 488-50) for GFP. The lasers were operated at low power densities (1 – 2 W/cm2), and
601 fluorescence was imaged with an Olympus IX71 inverted microscope with a 100x, 1.40-NA oil-
602 immersion objective and appropriate excitation, emission, and dichroic filters. A Photometrics
603 Evolve electron multiplying charge-coupled device (EMCCD) camera with > 90% quantum
604 efficiency captured the images at a rate of 20 frames per second. Each detector pixel corresponds
605 to a 49 nm × 49 nm area of the sample.
606
607 **Co-elution.** The interaction of TolC and colicin E1-T or -TR were determined by co-elution on
608 an SEC column. Purified TolC and colicin E1-T or -TR were mixed at a 1:2 molar ratio and
609 incubated at room temperature for 1 hour before loading onto a Superdex 200 Increase 10/300
610 GL column (GE Healthcare). The protein was eluted with 1.5 column volumes into 20 mM Tris
611 pH 8.0, 40 mM NaCl, 0.05% n-dodecyl-β-D-maltoside for colE1-T. For colE1-TR the NaCl
612 concentration was increased to 200 mM to prevent precipitation. Elution fractions were collected
613 every 0.5 mL. Peak fractions were concentrated to 20 µL and analyzed by 4-20% SDS-PAGE.
614
615 **Real-Time Efflux.** Real-time efflux activity in the presence of colE1-TR was determined as
616 previously described with some modifications[44,45]. Cells were resuspended to OD600 1.5 in cold
617 PBS with and without 10-100 µM colicin proteins and incubated for 15 minutes on ice. To turn
618 off efflux, 100µM carbonyl cyanide m-chlorophenyl hydrazone (CCCP) was added. After an
619 additional 15 minutes the efflux dye NNN was added to the cells to 10 µM. The cells were
620 incubated at 25 °C with shaking at 140 r.p.m. for 2 hours. Cells were harvested at 3,500 g for 5
621 minutes and washed once in 20 mM potassium phosphate buffer pH 7 with 1mM $MgCl_2$. Cell
622 concentrations were adjusted to OD600 1.0 and placed on ice. Then, 2 mL of the cell suspension
623 was loaded into a quartz cuvette (Agilent Technologies). Fluorescence was measured with an
624 Agilent Cary Eclipse fluorescence spectrophotometer with slit widths at 5 and 10 nm for
625 excitation wavelength of 370 nm and emission wavelength of 415 nm. Fluorescence
626 measurements were taken every 1 second. After 100 seconds, 50 mM glucose was added to re-
627 energize the cells and initiate efflux, and fluorescence data were collected for an additional 600
628 seconds.
629
630 **Minimum Inhibitory Concentrations (MICs).** MICs were determined using the broth dilution
631 method[55] with some modifications in 96 well plate format using LB media in 100 µL well
632 volumes. Cultures were grown at 37 °C with shaking at 250 r.p.m. and OD600 was read on a
633 Biotek plate reader after 20 hours. MICs are defined by the lowest concentration that prevents
634 visible growth. We chose an OD600 of >0.1 as the cutoff for growth. We report MICs as the
635 mean of 3 or 6 biological replicates with each replicate plotted (Figure 3D, Table S1). Due to the

636 2-fold discretized nature of concentration ranges used to determine MICs we do not report
637 statistical significance values as is typical of MIC reporting.
638
639 **Reconstitution of TolC into Amphipol.** Amphipol A8-35 (Anatrace) was solubilized in water at
640 33 mgs/mL. 1 mL of TolC at 0.5 mg/mL was mixed with 0.75 µL of A8-35 at 33 mg/mL for a 5-
641 fold weight excess and incubated at room temperature for 30 minutes. Bio-Beads SM-2 resin that
642 was washed in methanol and equilibrated with 20 mM Tris, 40 mM NaCl was added to the
643 reaction mixture at 0.5 g/mL to initiate detergent exchange for A8-35 and incubated with rotation
644 at 4 °C overnight. The mixture was transferred to a tube with fresh Bio-Beads and incubated at 4
645 °C for an additional 4 hours. The reaction mixture was loaded onto a HiLoad 16/60 Superdex
646 200 pg column on an ÄKTA Pure FPLC system and eluted with 1.5 column volumes in 20 mM
647 Tris pH 8.0, 40 mM NaCl to remove free A8-35 and detergent. For colicin-bound TolC in A8-35,
648 colicin E1-T was added to the reaction mixture at a >2 molar excess prior to gel filtration. TolC
649 or colicin-bound TolC in A8-35 was concentrated to 2-4 mg/mL for cryoEM.
650
651 **Reconstitution of TolC into lipid nanodiscs.** POPC (Avanti Polar Lipids) in chloroform was
652 dried under a stream of nitrogen and freeze dried to remove residual chloroform. Lipids were
653 reconstituted to 50 mM in cholate buffer (20 mM Tris pH 8.0, 100 mM NaCl, 0.5 mM EDTA,
654 100 mM cholate) in an amber glass vial. The vial was submerged under a stream of warm water
655 until the solution became clear. Lipids, membrane scaffold protein, and TolC were mixed in a
656 36:1:0.4 ratio as previously described[56]. Final concentrations were 4.5 mM POPC, 125 µM
657 MSP1D1, 50 µM TolC in a 2 mL reaction with cholate brought up to 20 mM and dodecyl-
658 maltoside up to 0.1%. The reaction mixture was incubated on ice for 1 hour. Bio-Beads SM-2
659 resin that was washed in methanol and equilibrated with 20 mM Tris, 40 mM NaCl were added
660 to the reaction mixture at 0.5 g/mL to initiate nanodisc formation and incubated with rotation at
661 4°C overnight. The mixture was transferred to a tube with fresh Bio-Beads and incubated at 4 °C
662 for an additional 4 hours. The reaction mixture was loaded onto a HiLoad 16/60 Superdex 200
663 pg column on an ÄKTA Pure FPLC system and eluted with 1.5 column volumes in 20 mM Tris
664 pH 8.0, 40 mM NaCl to separate TolC inserted into nanodiscs from empty nanodiscs. For
665 colicin-bound TolC in nanodiscs, colicin E1-T was added to the reaction mixture at a >2 molar
666 excess prior to gel filtration. TolC or colicin-bound TolC in nanodiscs was concentrated to 2-4
667 mg/mL for cryoEM.
668
669 **Cryoelectron microscopy.** 3 µL of protein solution (TolC/colE1-T in amphipol or TolC/colE1-T
670 in nanodiscs) was diluted to approximately 1.05 mg/mL concentration, applied to a glow-
671 discharged TEM grid, and plunge-frozen in ethane using a Vitrobot Mark IV (FEI Company)
672 with grade 595 filter paper (Ted Pella). Glow discharge was performed in ambient atmosphere at
673 0.39 mBar pressure. Imaging was performed using a Talos Arctica (FEI Company) operated at
674 200 kV with energy-filter and K2 Summit (Gatan, Inc.) for detection. To collect multiple images
675 per hole while maintaining parallel illumination conditions, a nonstandard 20 µm condenser
676 aperture was used to image TolC-colE1-T in nanodiscs. At nominal magnification of 205,000×,
677 images were acquired in counting mode with a calibrated pixel size of 0.6578 Å. Fresnel fringes
678 attributable to the beam interaction with the aperture were often seen in images. Some
679 investigators have moved the microscope stage and altered the nominal objective lens true focus
680 point to generate a fringe-free condition[57]. In this study, imaging at 205,000× with a 20 µm
681 aperture yielded better results than imaging at 130,000× with a 50 µm aperture; at 130,000× with

682 a 20 µm aperture the fringes were extremely severe due to the larger field of view, so a full
683 dataset was not collected with those conditions. TolC in nanodiscs (without colE1-T) was
684 imaged at 130,000× with a 50µm condenser aperture (Table S2).
685
686 Micrographs were collected with SerialEM[58] using in-house modifications of the scripts of Chen
687 Xu (sphinx-emdocs.readthedocs.io). Briefly, multishot imaging was configured with 4 images
688 per hole for each of 16 holes; intermediate-magnification montages of grid squares were
689 acquired; points were selected manually for collection of 64 images per point; images were
690 acquired using coma-compensated image shift as gain- and dark-corrected LZW-compressed
691 TIFs. Side, top, and oblique views were seen in areas of thin ice. During screening, ice thickness
692 was estimated at 17-30nm by the method of I_0/I_{ZLP}[59].
693
694 The collection of micrographs of TolC without colicin at 130,000× magnification has been
695 previously described[60].
696
697 **3D reconstruction and modeling.** Final reconstructions were obtained using cryoSPARC 2[61].
698 1,018 micrographs were collected of amphipol-embedded TolC/colE1-T. Micrographs were
699 motion-corrected using RELION 3[62]. CTF parameters were determined by means of *ctffind*[63].
700 115,362 particles were selected with crYOLO[64]. 2D classification revealed that many particles
701 had aberrant morphology and only 24,624 (21%) were selected for 3D reconstruction. *Ab initio*
702 reconstruction in cryoSPARC 2[61] was effective at recovering a map whose shape was similar to
703 that of previously described TolC trimers. However, the data could only be refined to a nominal
704 global resolution of 6.0 Å, and lumenal density was insufficiently resolved. 4,492 micrographs
705 were then collected of nanodisc-embedded TolC/colE1-T and processed similarly. Of the
706 339,779 particles detected by cryoSPARC Live, 179,834 (53%) were in good classes. Although
707 there were slightly fewer particles per micrograph in the nanodisc dataset, more particles per
708 micrograph were usable. Beginning with the *ab initio* model and mask derived from the
709 amphipol data, this particle set was refined by cryoSPARC 2 non-uniform refinement with or
710 without imposed C_3 symmetry. The maps refined to nominal global resolutions of 2.81 Å and
711 3.09 Å for the symmetrized and asymmetric maps, respectively. There was local variation in
712 resolution within the map, with consistent, high resolution in the middle of TolC and lower
713 resolution at the lids and for colE1-T. Local resolution was computed in cryoSPARC by the
714 locally windowed FSC method[65] and rendered with UCSF Chimera. To reduce the voxel-based
715 values to averages for four regions of the complex, the local resolution map was masked to
716 include only voxels within 3 Å of a modeled atom and then the median value was calculated for
717 those voxels closest to colE1, closest to TolC residues 168-172 and 386-390, closest to TolC
718 residues 285-301 and 76-82, or closest to other TolC residues. Furthermore, it is notable that
719 while the nanodisc appears as a double-belt in the symmetrized map, in the asymmetric map the
720 nanodisc protein mostly appears on the side of TolC that is bound to colE1-T. One possible
721 explanation is that, despite masking, nanodisc asymmetry is a confounder of the asymmetric
722 refinement and is one source of heterogeneity in the data. Another possibility is that the C-
723 terminus of colE1-T forms an interaction with the nanodisc, causing preferential alignment of the
724 nanodisc with respect to the TolC/colE1-T complex.
725

196,158 particles of TolC without colicin were obtained as previously described[60]. Homogeneous refinement yielded a structure at 2.89 Å; local motion correction and global CTF refinement yielded a final map at 2.84 Å.

Modeling was initiated by rigidly docking a crystal structure of TolC in complex with hexamminecobalt (1TQQ)[27] into the symmetrized map density. Automated, semi-automated, and manual real-space refinement was performed using phenix[66], ISOLDE[67], and coot[68]. For TolC with colE1-T, additional refinement was performed in AMBER using the cryoEM density map as a restraint.

Although additional residues are present at the TolC C-terminus, these were not modeled because the density becomes unsharp after residue 428. Blurred density in the map suggests that the C-terminus follows helix 3 towards the periplasmic end of the molecule. ColE1-T was modeled *ab initio*. The 3-fold symmetrized map contains density at ~1/3rd occupancy for colE1-T and this density contains some high-resolution information not present in the asymmetric map, except near the TolC lid regions where symmetrization overlays colE1-T density with TolC density at a threefold-related position. First, polyalanine helices were placed in the helical density in coot. Cross-correlation coefficients for both helices are higher with the N-terminus oriented towards the periplasm, and the Christmas tree appearance was observed indicating that this is the correct chain orientation. An estimate of the registration was made by visual inspection of potential anchor residues. Finally, the hinge region was filled in using phenix and coot. This completed chain was refined against the asymmetric map in ISOLDE. Iteration between phenix, coot, and ISOLDE was continued until acceptable fit to density was achieved. In the case of TolC with colE1-T, the map was further improved by combining map information with molecular dynamics force fields[31]. Briefly, starting with the phenix/coot/ISOLDE-refined model, we performed restrained simulated annealing in AMBER, heating from 0K to 300K for 0.2 nsec, holding constant temperature for 1 nsec, and then cooling to 0K over 0.2 nsec. The cryoEM density map is utilized as a restraint potential in the annealing so that both map information and AMBER force field information are simultaneously utilized to obtain an optimum model consistent with the data[31]. The protein force field used the ff14SB force field[69] and a generalized Born implicit solvent model with *igb=8*[70], and a nonbonded cutoff of 20 Å. The relative weight of real-space map-based restraints and the force field was fixed using *fcons=0.02*. For colE1-T, information from the symmetrized map was integrated into the modeling procedure during manual remodeling in coot, but map-based refinement in phenix, ISOLDE, and AMBER were against the asymmetric map. TolC without colE1-T was modeled similarly but using the TolC-colE1-T structure as a starting point instead of 1TQQ, and without final AMBER refinement.

Molecular representations were generated with Chimera, ChimeraX[71] or PyMOL (Schrödinger, LLC).

766

767 **Supplemental Information**

768

769

770 **Colicin E1 binds to TolC as an open hinge to penetrate the outer-membrane**

771

772 S. Jimmy Budiardjo, Jacqueline J. Stevens, Anna L. Calkins, Ayotunde P. Ikujuni, Virangika K.
773 Wimalasena, Emre Firlar, David A. Case, Julie S. Biteen, Jason T. Kaelber and Joanna S.G.
774 Slusky

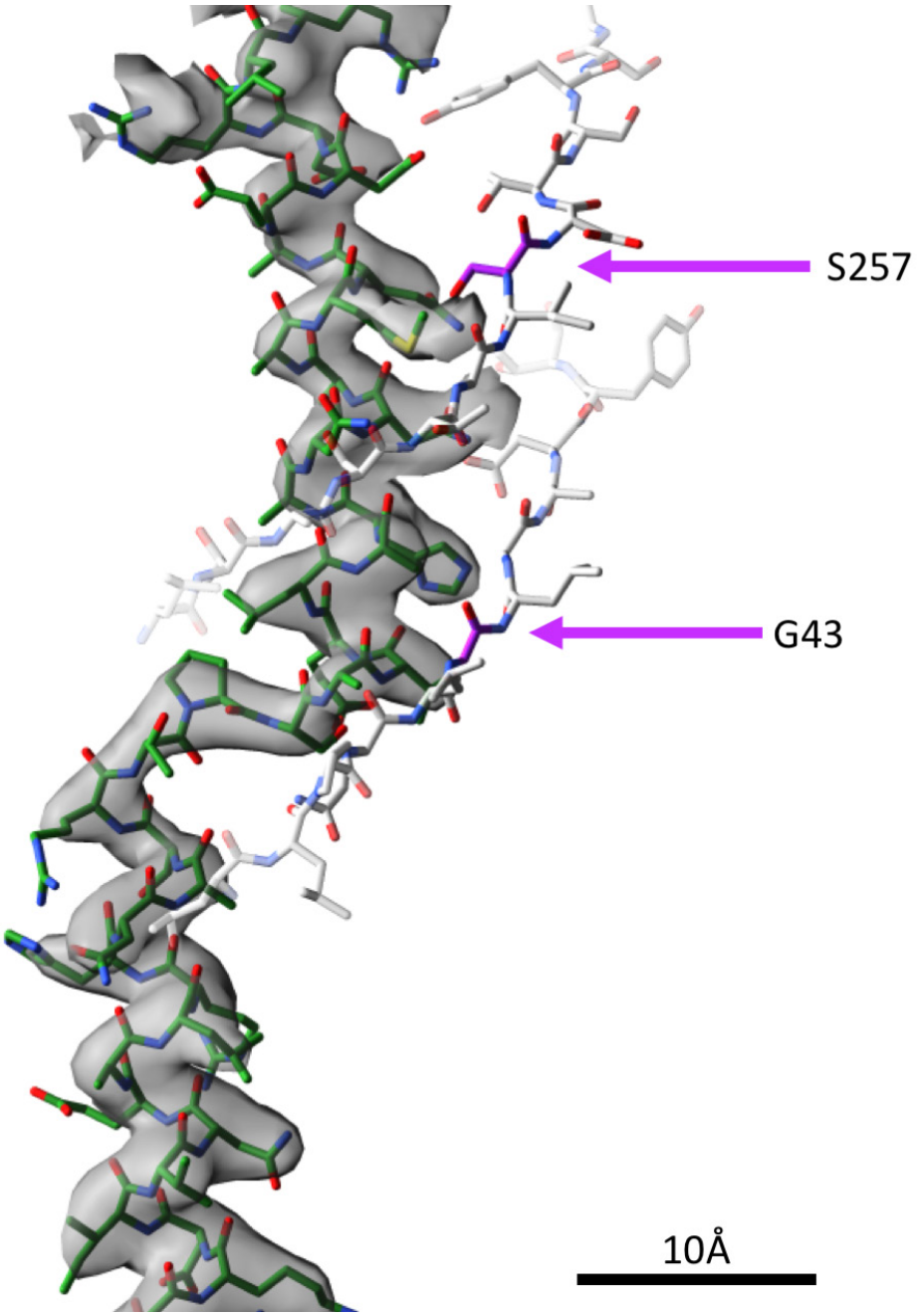

Figure S1. TolC box density cropped from the fully asymmetric cryoEM map of the TolC/colE1-T complex. Mutations at positions G43 and S257 in the TolC (grey sticks) barrel make direct contact with colE1-T (green). These mutations were previously shown to abolish WT colE1 function[34]. Mutations to bulkier side chains introduce a steric clash that prevents binding.

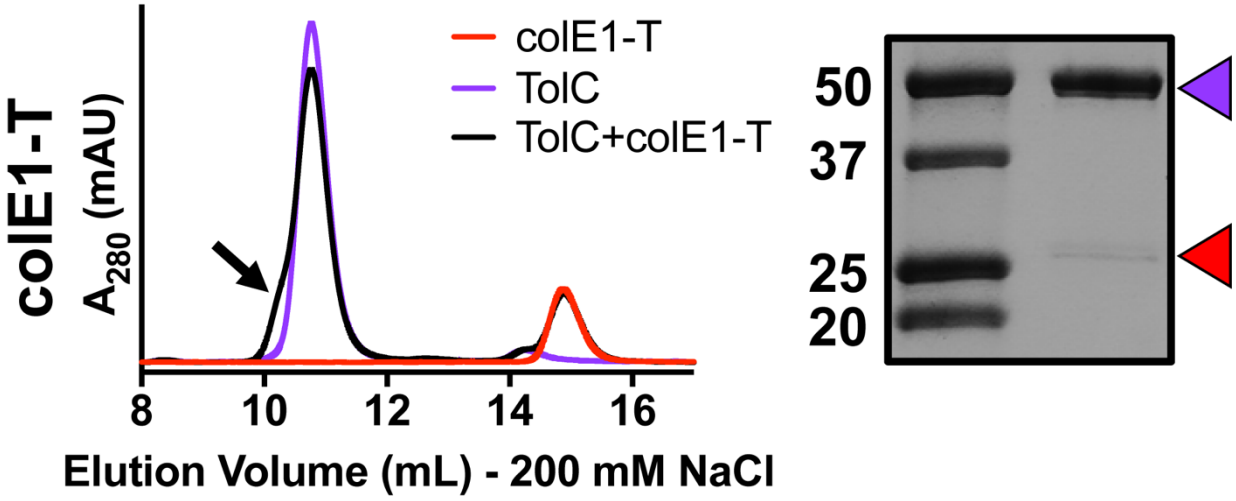

783

784 **Figure S2. Co-elution of colE1-T with TolC at 200 mM NaCl (black).** Under this higher salt
785 concentration, when TolC (purple) and colE1-T (red) are mixed, there is a smaller peak shift than
786 that seen with colE1-TR and the presence of a shoulder (black arrow). SDS-PAGE of the
787 shoulder shows presence of both TolC (purple arrow) and colE1-T (red arrow). Although some
788 binding was detected, this higher salt concentration prevents full binding as indicated by a much
789 fainter band for colE1-T than seen at the lower salt concentration (Figure 4A).

790

791

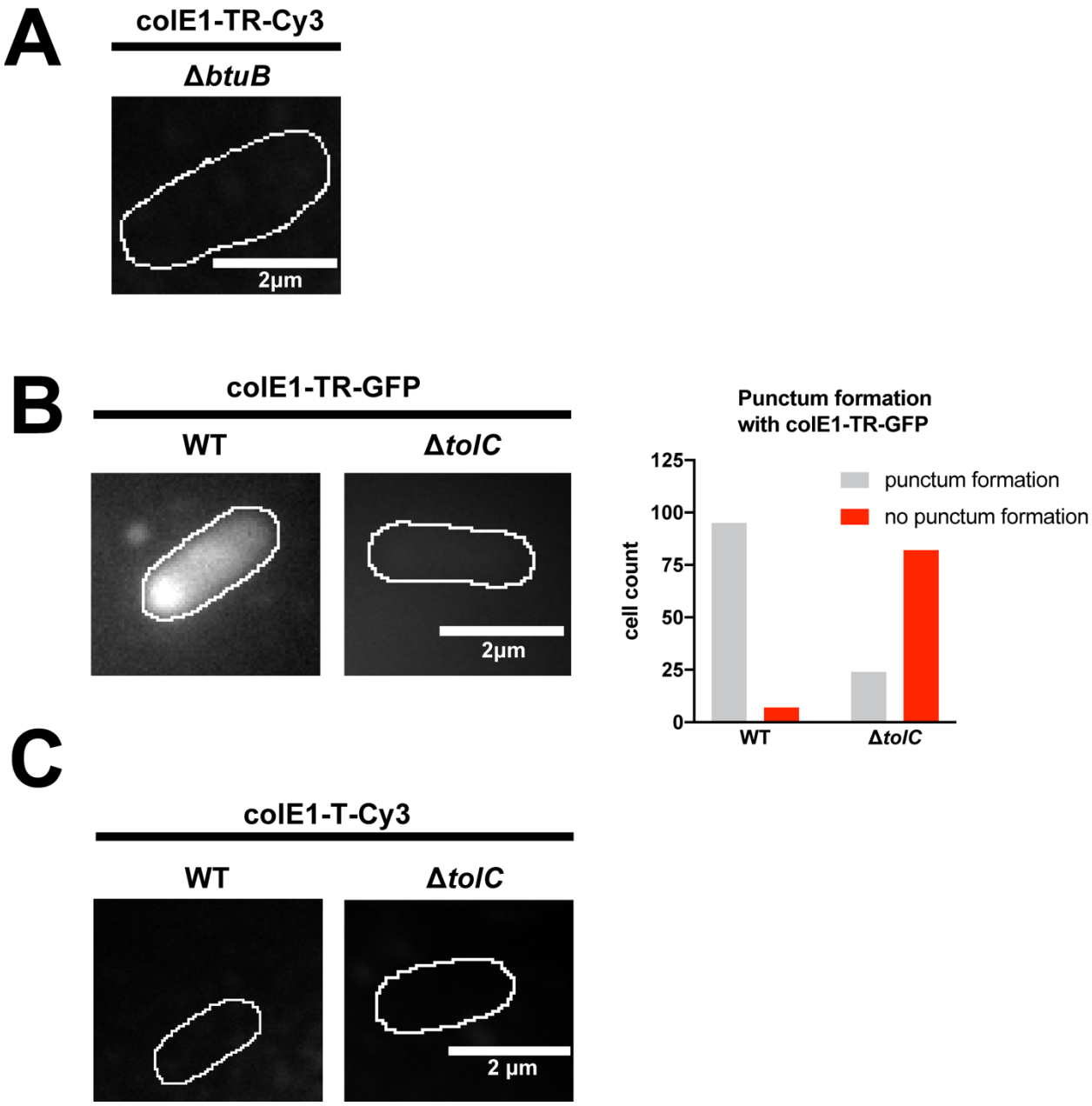

Figure S3 Single-molecule microscopy. Fluorescence images overlaid on outlines of living *E. coli* cells from phase-contrast microscopy for WT and Δ*tolC* for colE1-TR-GFP and counts of cells where colE1-TR-GFP punctum formation was observed. (A) 97% of cells showed no binding of Cy3-labeled colE1-TR to Δ*btuB* (B) ColE1-TR-GFP forms similar puncta as Cy3-labeled ColE1-TR (main text Figure 4C). (C) No binding of Cy3-labeled colE1-T to WT or Δ*tolC* cells was detected with Cy3-labeled colE1-T. Scale bars: 2 μm.

805
806

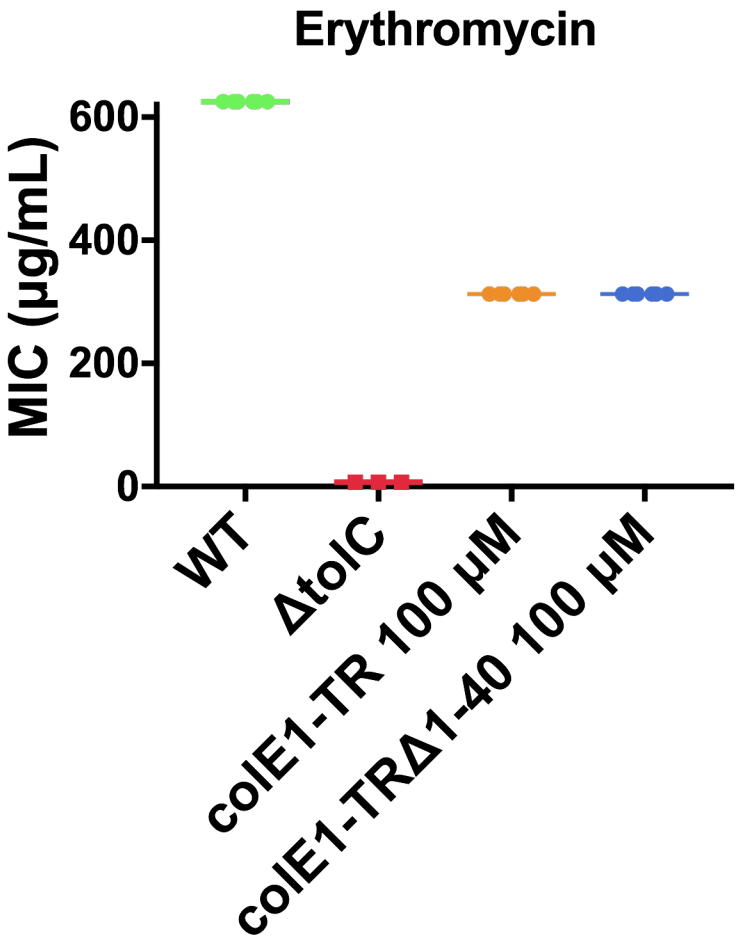

807

808

809 **Figure S4. Minimum Inhibitory Concentration of Erythromycin with colE1-TR TolA box**
810 **deletion construct.** The MIC for erythromycin with 100 µM colE1-TR or colE1-TR$_{\Delta 1\text{-}40}$ is
811 identical indicating that TolA engagement by colE1-TR does not contribute to antibiotic
812 susceptibility.

813

814
815
816

817 **Table S1.**

818 Mean minimum inhibitory concentrations (MICs) of antimicrobials in the presence of colE1-TR.

819

	Erythromycin (μg/mL)	Ciprofloxacin (ng/mL)	Kanamycin (μg/mL)	Benzalkonium Chloride (μg/mL)
WT	**625.00**	**56.25**	**21.88**	**45.83**
Δ*tolC*	**7.03**	**15.63**	**NA**	**6.88**
WT + 10 μM colE1-TR	**364.58**	**75.00**	**28.14**	**25**
WT + 100 μM colE1-TR	**312.50**	**28.13**	**6.25**	**6.25**

820

821

822 **Movie S1.**

823 A representative 8-second clip of colE1-TR bound to a live cell. ColE1-TR localizes on, and
824 remains bound to, the extracellular surface of *E. coli*. Fluorescence movie of Cy3-labeled colE1-
825 TR on living WT *E. coli* overlaid on outline of the *E. coli* cell from phase-contrast microscopy.
826 Continuous imaging at 25 frames per second. Scale bar: 2 μm.
827
828